CYTOSKELETON

Transition of human γ-tubulin ring complex into a closed conformation during microtubule nucleation

Cláudia Brito[1]†, Marina Serna[2]†, Pablo Guerra[3], Oscar Llorca[2]*, Thomas Surrey[1,4,5]*

Microtubules are essential for intracellular organization and chromosome segregation. They are nucleated by the γ-tubulin ring complex (γTuRC). However, isolated vertebrate γTuRC adopts an open conformation that deviates from the microtubule structure, raising the question of the nucleation mechanism. In this study, we determined cryo–electron microscopy structures of human γTuRC bound to a nascent microtubule. Structural changes of the complex into a closed conformation ensure that γTuRC templates the 13-protofilament microtubules that exist in human cells. Closure is mediated by a latch that interacts with incorporating tubulin, making it part of the closing mechanism. Further rearrangements involve all γTuRC subunits and the removal of the actin-containing luminal bridge. Our proposed mechanism of microtubule nucleation by human γTuRC relies on large-scale structural changes that are likely the target of regulation in cells.

Microtubules are protein filaments consisting of alpha and beta (α/β)–tubulin heterodimers that associate longitudinally into straight protofilaments that arrange into a tube (*1*–*3*). Protofilaments interact laterally with a slight offset, giving rise to a pseudo-helical lattice symmetry with a rise of three tubulin monomers per turn. There is one lateral protofilament interface, called the seam, with lateral α-β instead of the usual α-α– and β-β–tubulin contacts (*4*). Microtubules grown in vitro from purified tubulin are well known for their polymorphism, growing with a variety of different protofilament numbers (*5*) or even as sheets (*6*). In cells, however, microtubules are always tubular, and their protofilament number is precisely controlled (*7*). In humans and most other organisms, cytoplasmic microtubules always consist of exactly 13 protofilaments (*8*), which ensures that these tracks for motor proteins are perfectly parallel to the microtubule axis (*9*). One key element controlling microtubule morphology in cells is the process of microtubule nucleation that is typically mediated by the main nucleator γ-tubulin ring complex (γTuRC) (*10*, *11*), which is thought to serve as a template for the early steps of microtubule growth (*12*–*17*).

γTuRC is a ~2.2 MDa cone-shaped protein complex that arranges 14 γ-tubulins in a helical manner. The γ-tubulins are held in place by γ-tubulin complex proteins (GCPs) that interact laterally, forming the base of the cone (*18*–*20*). In budding yeast, two structurally homologous GCPs exist, GCP2 and GCP3 (*21*, *22*), that alternate in the wall of the cone (*19*, *23*). The composition of vertebrate γTuRC is more complex (*24*–*26*). Recent cryo–electron microscopy (cryo-EM) structures of human and *Xenopus* γTuRC revealed that two adjacent GCP2/3 pairs are replaced by a GCP4/5 pair and a GCP4/6 pair, and that a "luminal bridge" is positioned inside the cone (*27*–*30*). This bridge contains an actin-like molecule and two copies of mitotic-spindle organizing protein 1 (MZT1) and the N-terminal extensions (NTEs) of one GCP3 and GCP6, forming MZT1/3NTE and MZT1/6NTE modules (*31*), which have been proposed to be important for complex assembly and stability (*32*–*34*). The function of the actin-like molecule in the γTuRC is less understood, much like the unclear role of an "end protrusion" that extends from the last GCP3 on the outside of the complex, possibly representing another MZT1-like/NTE module (*28*–*31*, *35*).

The γ-tubulins held by GCP2/3 in positions 1 to 8 roughly match the structure of a 13-protofilament microtubule. However, the part of the complex containing metazoan-specific GCP4/5 and GCP4/6 and a final GCP2/3 pair in positions 9 to 14 adopts an open conformation, causing the positions of their corresponding γ-tubulins to deviate from the helical path of the α/β-tubulins in a microtubule, exposing all 14 γ-tubulins (*27*–*30*). This conformation is distinct from that of yeast γTuRC, which is more closed, causing the last γ-tubulin to be positioned above the first, leaving 13 γ-tubulins exposed to serve as a template for the nucleation of a 13-protofilament microtubule (*19*, *23*). The pronounced structural deviation of one half of vertebrate γTuRC from the microtubule structure is thought to explain its low nucleation efficiency when purified (*27*, *34*, *36*). A conformational change from this open and likely inactive to a more closed and likely functional structure may be required for vertebrate γTuRC to act as a template for the nucleation of a 13-protofilament microtubule. This change may be either induced by an allosteric regulator or by the nucleating microtubule itself. High-resolution structures of γTuRC nucleating a microtubule would help explain how this transition occurs.

Efficient nucleation of very short microtubules by γTuRC

To be able to determine the cryo-EM structure of human γTuRC in its microtubule nucleating state, we needed to drastically increase the nucleation efficiency of the purified complex. We found that a slowly guanosine triphosphate (GTP)–hydrolyzing, but otherwise normally growing, tubulin variant in which the catalytic glutamate in α-tubulin is replaced by an aspartate [recombinant human E254D (Glu^{254}→Asp) mutant (*37*)] considerably stimulated the nucleation efficiency of purified human γTuRC in vitro (Fig. 1A and movie S1). Microtubules that were nucleated from surface-immobilized γTuRC were visualized by total internal reflection fluorescence (TIRF) microscopy using fluorescently labeled end-binding protein EB3 that accumulates at growing microtubule ends and weakly binds all along microtubules (*37*, *38*). γTuRC-mediated microtubule nucleation increased with the concentration of E254D tubulin (Fig. 1, B and C), displaying the typical power law dependence previously observed for wild-type mammalian tubulin (*12*, *27*, *34*, *36*). The γTuRC-mediated microtubule nucleation rate could be increased by ~2 orders of magnitude compared with nucleation in the presence of wild-type tubulin (Fig. 1D; and see methods in the supplementary materials). Approximately 10% of γTuRCs nucleated microtubules within 5 min as compared with only ~0.1% with wild-type tubulin (see methods). The smaller exponent of the power law fit suggested that the nascent microtubule (also called the critical nucleus) required for microtubule nucleation to occur is smaller for the more slowly GTP-hydrolyzing tubulin (Fig. 1D), suggesting a mechanistic explanation for accelerated nucleation.

To keep γTuRC-nucleated microtubules as short as possible for cryo-EM observation, we added the microtubule plus-end capping designed ankyrin repeat protein (DARPin) $(D1)_2$ (*39*). This plus-end capper slowed down the plus-end growth speed of E254D microtubules, either grown from stabilized microtubule seeds (fig. S1, A and B) or nucleated from γTuRC (Fig. 2, A and B) in a $(D1)_2$ concentration–dependent manner up to an almost complete stop in growth, in agreement with previous observations with wild-type microtubules (*39*). In addition to slowing down growth, which leads to shorter EB3 comets at growing microtubule ends (*40*, *41*), $(D1)_2$ unexpectedly further increased the nucleation efficiency of γTuRC, as demonstrated

[1]Centre for Genomic Regulation (CRG), The Barcelona Institute of Science and Technology, Barcelona, Spain. [2]Structural Biology Programme, Spanish National Cancer Research Centre (CNIO), Madrid, Spain. [3]Cryo-Electron Microscopy Platform–IBMB CSIC, Joint Electron Microscopy Center at ALBA (JEMCA), Barcelona, Spain. [4]Universitat Pompeu Fabra (UPF), Barcelona, Spain. [5]Catalan Institution for Research and Advanced Studies (ICREA), Barcelona, Spain.
*Corresponding author. Email: ollorca@cnio.es (O.L.); thomas.surrey@crg.eu (T.S.)
†These authors contributed equally to this work.

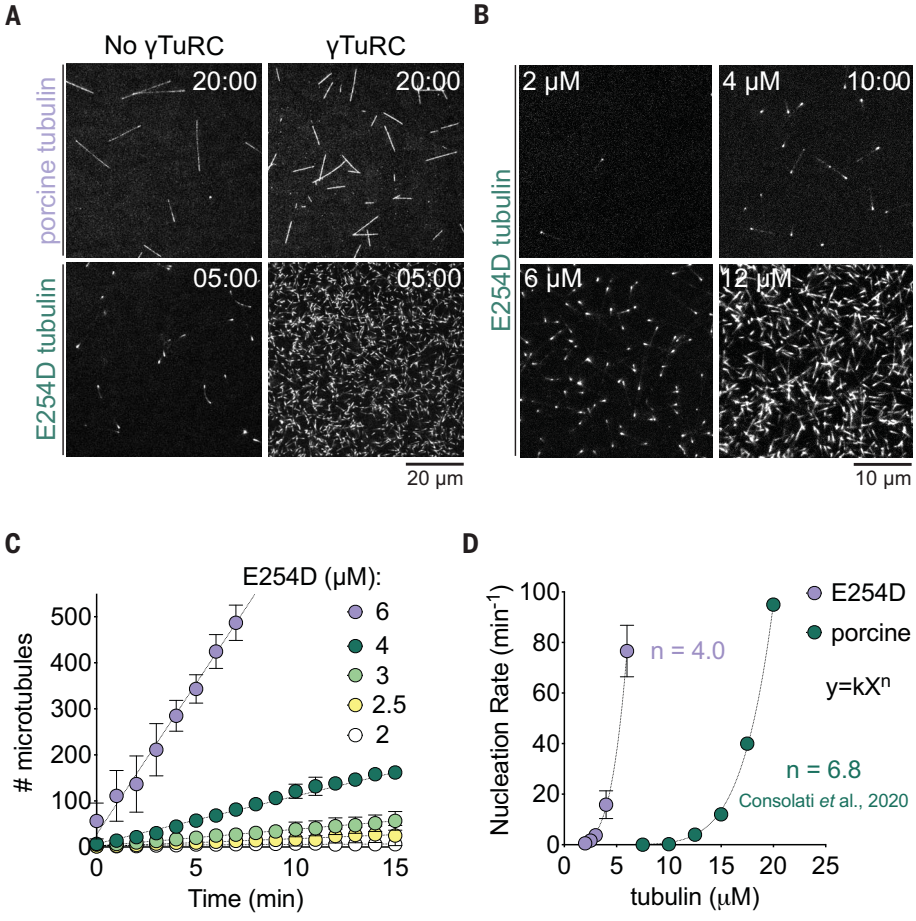

Fig. 1. E254D tubulin promotes γTuRC-mediated microtubule nucleation. (**A**) TIRF microscopy images of few spontaneously nucleated microtubules in the absence of immobilized γTuRC (left) and microtubules nucleated by immobilized γTuRC (right) in the presence of 12 μM (top) porcine tubulin (CF640R-labeled, 5.4%) or (bottom) E254D tubulin and 20 nM mGFP-EB3, 5 or 20 min after starting imaging. Surface-immobilized γTuRC (1 nM used for immobilization) is not shown. (**B**) TIRF microscopy images of γTuRC-nucleated microtubules in the presence of 2, 4, 6, and 12 μM E254D tubulin and 20 nM mGFP-EB3, 10 min after starting imaging. Surface-immobilized γTuRC is not shown. (**C**) Number of microtubules nucleated over time. Dots represent mean values, error bars are SEM. For symbols without visible error bars, error bars are smaller than the symbol size. The lines represent linear regressions. Data for plots were pooled from at least two independent experiments. Number of microtubules analyzed per condition: 6 μM, *n* = 1663; 4 μM, *n* = 379; 3 μM, *n* = 298; 2.5 μM, *n* = 143; 2 μM, *n* = 26. (**D**) Nucleation rates calculated from the slope of the linear regression in (C). Dots represent mean values, error bars are SEM. For symbols without visible error bars, error bars are smaller than the symbol size. The dashed lines represent the fit to a power law function. Data for porcine tubulin, as published previously (*27*), are shown for comparison with E254D tubulin data.

by the increase in the number of EB3-labeled growing microtubule plus ends (Fig. 2, A and C, and movie S2). The nucleation rate increased nonlinearly with $(D1)_2$ concentration (Fig. 2D), possibly as a consequence of preventing the disassembly of nascent microtubules forming on the γTuRC. More than 90% of γTuRCs nucleated a microtubule within 5 min (see methods).

We further optimized the nucleation conditions by cryo-EM using the mixture of E254D tubulin and $(D1)_2$ to obtain γTuRC-nucleated microtubules with lengths of ~100 nm (fig. S2). All microtubules displayed one γTuRC-capped end and one open end. At the highest $(D1)_2$ concentrations used, many γTuRC-nucleated microtubules showed only a few or just a single tubulin layer on the γTuRC (fig. S2, bottom). Essentially all γTuRCs appeared to be nucleating (fig. S2, bottom).

Cryo-EM reveals several stages of γTuRC closure during microtubule nucleation

γTuRC-nucleated microtubules were analyzed by cryo-EM, and more than 1.5 million particles were initially selected and subjected to single-particle image processing (fig. S3 and table S1). Two-dimensional (2D) averages illustrated side views of short microtubules with γTuRC capping one of the ends, as well as partially tilted views with a circular shape and protofilaments projecting from γTuRC (fig. S3A). Initial 3D refinement steps converged into a consensus structure of the microtubule nucleating γTuRCs at an overall resolution of ~4 Å. Deep learning–based classification and 3D variability analysis (see methods) (*42*, *43*) of the cryo-EM data organized a continuum of nucleating γTuRC structures, wherein microtubule nucleating γTuRCs displayed a range of increasingly closed conformations as the length of the nucleated microtubule increased (Fig. 3A). No γTuRC complexes were detected that had not started to nucleate a microtubule. The major components of heterogeneity corresponded to the positioning and length of the protofilaments, the degree of closure of γTuRC, and the presence or absence of the previously noted density in the cryo-EM map extending from GCP3 in position 14 (*28*–*31*, *35*), which appeared to help to close the complex like a "latch" (fig. S4 and movies S3 and S4).

Cryo-EM maps corresponding to two major stages of conformational closure of γTuRC were obtained using particle analysis and classification algorithms (fig. S3B; and see methods) (*44*, *45*). The most prominent conformation preserves the previously described γTuRC stoichiometry and GCP arrangement, together with 13 α/β-tubulin protofilaments extending from the complex (Fig. 3B). GCP3 in position 14 is placed just above γ-tubulin in position 1 (Fig. 3B), reminiscent of yeast γTuRC (*19*, *23*), implying the closure of the human complex with respect to its open conformation (Fig. 3C and movie S5). 2D averages of the particles assigned to this conformation reveal that protofilaments are relatively short (Fig. 3D, 2D average), and these particles could be mapped back to short γTuRC-nucleated microtubules in the movies (fig. S3B). In this conformation, some protofilaments do not have established full lateral contacts yet (Fig. 3D, arrowhead). We infer that this conformation is not fully closed and corresponds to an earlier stage of γTuRC-mediated microtubule nucleation, hereafter referred to as the early closed conformation. We also obtained a cryo-EM map of a fully closed conformation of γTuRC bound to longer protofilaments with fully established lateral contacts (Fig. 3E, arrowhead), suggesting that this conformation corresponds to a later stage after nucleation is completed (movie S4). 2D averages of the particles in the fully closed conformation reveal longer protofilaments (Fig. 3E, 2D average), and these particles correspond to longer γTuRC-nucleated microtubules in the movies (fig. S3B). Together, the cryo-EM maps of microtubule nucleating γTuRC reveal the conformational transitions that transform the open conformation of γTuRC before nucleation into a fully closed conformation after it has nucleated a microtubule.

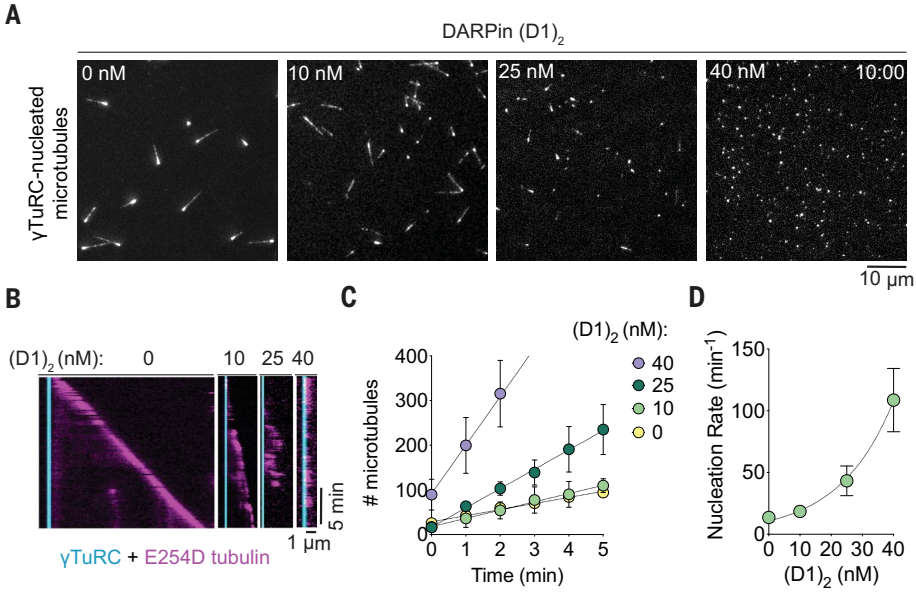

Fig. 2. DARPin caps the plus ends of γTuRC-nucleated microtubules. (**A**) TIRF microscopy images of γTuRC-nucleated microtubules in the presence of 4 μM E254D tubulin, 20 nM mGFP-EB3, and in either the absence (leftmost panel) or presence of DARPin $(D1)_2$ at the indicated concentrations. Surface-immobilized γTuRC (1 nM used for immobilization) is not shown. (**B**) Representative kymographs of γTuRC-nucleated E254D microtubules in the absence (leftmost panel) and presence of DARPin $(D1)_2$ at the indicated concentrations, 4 μM E254D tubulin, and 20 nM mGFP-EB3 (magenta). For immobilization, 1 nM γTuRC (cyan) was used. (**C**) Number of microtubules nucleated over time for the conditions in (A). Dots represent mean values, error bars are SEM. For symbols without visible error bars, error bars are smaller than the symbol size. The lines represent linear regressions. Data for plots were pooled from at least two independent experiments. Number of microtubules analyzed per condition: 40 nM, n = 826; 25 nM, n = 470; 10 nM, n = 219; 0 nM, n = 282. (**D**) Nucleation rates calculated from the slope of the linear regression in (C). Dots represent the mean values, error bars are SEM. For symbols without visible error bars, error bars are smaller than the symbol size. The dashed line represents a fit to the data using an exponential growth equation.

Closure of human γTuRC leaves 13 γ-tubulins accessible for protofilament elongation

The 3.9-Å resolution cryo-EM map of the early closed conformation allowed us to identify and model the structure of all GCPs and γ-tubulins in the γTuRC and most of the first layer of the α/β-tubulins (positions 1 to 9) (Fig. 4A and fig. S5A), excluding most of the NTEs of the GCP subunits, where resolution was insufficient or some regions of the NTEs were not visible (see methods). Local resolution for most GCPs was between 3.5 and 4 Å and allowed the identification of sequences specific for each GCP subunit (fig. S5, B to D). The γ-tubulin in position 1 is blocked from adding an α/β-tubulin by GCP3 in position 14 (Fig. 4A, right panel). The other 13 γ-tubulins at positions 2 to 14 are all bound to a α/β-tubulin heterodimer, representing the bottom layer of a 13-protofilament microtubule (Fig. 4A).

Comparison of the structure of the early closed conformation of γTuRC with the structure of open γTuRC revealed conformational changes in all GCP subunits that promote the closure of the γTuRC ring during microtubule nucleation (Fig. 4B; fig. S6, A and B; and movie S5). After aligning both structures at position 1, superimposing the two cryo-EM maps showed a remarkable movement of GCP3 in position 14 toward position 1 in the early closed conformation of γTuRC (Fig. 4B). Closure encompasses coordinated conformational changes of the N-terminal domains of each GCP subunit (GCP N-GRIP), from a kinked to a straighter conformation (Fig. 4C and fig. S6C). This concerted straightening allows accommodation of all γ-tubulin–GCP subunits in the more restricted space of the closed γTuRC (fig. S6B).

Structural rearrangements at the seam position and in the lumen of γTuRC participate in closure

The density protruding from GCP3 at position 14 of the open γTuRC, previously proposed to be an MZT1-like/NTE module (*28*–*31*, *35*), was also visible in the early closed conformation of γTuRC (Fig. 4D). Although resolution of this density in the cryo-EM map was not sufficient for model building because of its flexibility (fig. S4), the structure suggests that this module at position 14 contributes to initiate γTuRC closure by establishing contacts with γ-tubulin in position 1 and also α-tubulin in position 2, similar to a latch (Fig. 4D). This arrangement implies that the incorporation of α/β-tubulin heterodimers at the base of the microtubule seam (position 2 in γTuRC) is required to promote the closing of γTuRC, rationalizing why γTuRC shows an open conformation with 14 exposed γ-tubulins when it has not nucleated yet but adopts a 13-fold symmetry once starting to nucleate a microtubule.

The early closed conformation of γTuRC nucleating a microtubule also contained a luminal density (Fig. 4E), most of which fits the previously described MZT1/NTE modules of the luminal bridge in open γTuRC (fig. S7A). The density for the actin-like molecule could not be detected at its place, although some scattered density was still present in the vicinity (fig. S7B). A systematic search for actin in this region using strategies such as focused classifications and density subtraction was unsuccessful (fig. S7C). We infer that actin has been lost in the early closed conformation or, alternatively, has moved to a different location where it is flexibly attached and thus it cannot be averaged.

The fully closed conformation of γTuRC matches the structure of a 13-protofilament microtubule

The fully closed conformation of the microtubule nucleating γTuRC was less abundant in our dataset, resulting in a cryo-EM map at an average resolution of 4.4 Å with several regions at resolutions inadequate for model refinement but nevertheless sufficient to unambiguously identify all GCP subunits. Fitting the structure of the early closed conformation within the cryo-EM map of the fully closed conformation illustrates how some of the α/β-tubulin heterodimers change position in the fully closed conformation (Fig. 5A) and establish lateral contacts that were still missing at some protofilament interfaces in the early closed conformation (Fig. 3, D and E).

In the fully closed conformation, the latch density was not detected anymore (Fig. 3E and fig. S4, A to C), which suggests that it is only necessary to assist in initiating closure. Once fully closed, the contacts between the GCP subunits and between the protofilaments may be sufficient to maintain the closed state. Accordingly, density for the conserved loops in α/β-tubulin dimers that stabilize lateral contacts between protofilaments is observed for some protofilaments in the early closed conformation but is clearly visible for all protofilaments in the fully closed conformation in focused refined maps (fig. S8, A and B). In addition, the resolution of the cryo-EM map of the early closed conformation was sufficient to detect guanosine diphosphate in every γ-tubulin in the early closed conformation (fig. S8C). Neither the MZT1/NTE modules nor the actin were detected in the lumen of the fully closed conformation (Fig. 5B), suggesting that the luminal bridge is incompatible with the full closure of the complex.

Flexibly fitting the structure of the early closed conformation into the cryo-EM density of the

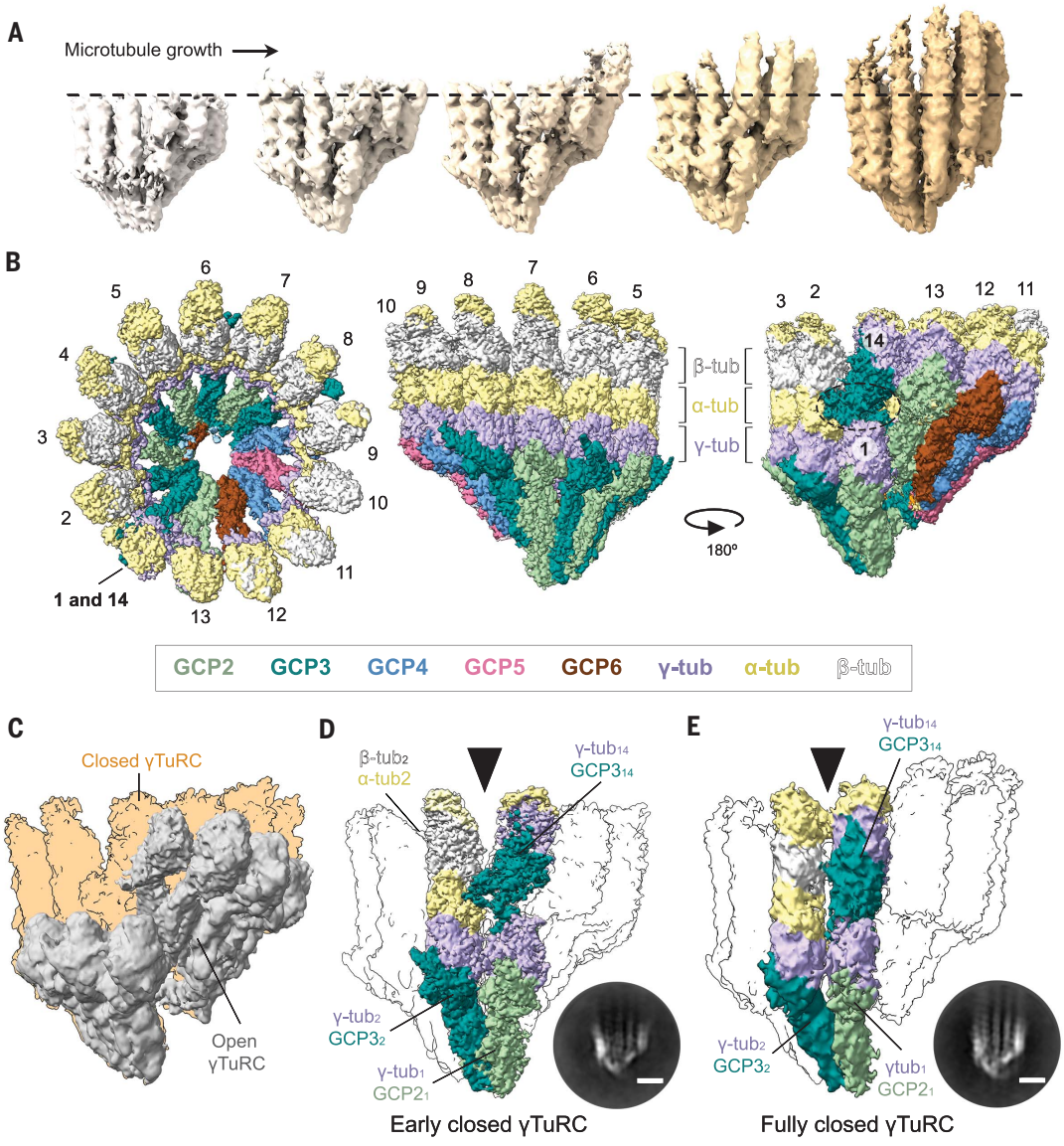

Fig. 3. γTuRC-nucleated and DARPin-capped E254D microtubules visualized by cryo-EM. (**A**) Representative 3D reconstructions generated from cryo-EM data of the microtubule nucleating γTuRC obtained by heterogeneity analysis. Maps represent a continuum of the microtubule nucleation process, from the initial nucleation stages to microtubule elongation (from left to right). (**B**) Top (left panel) and two side views (middle and right panels) of the cryo-EM map for microtubule nucleating γTuRCs in their early closed conformation, color coded as indicated. (**C**) Side view comparison of the cryo-EM maps for the early closed (cartoon, orange) and the open (surface, gray; EMD-11888) conformation of γTuRC. (**D** and **E**) Side views of the cryo-EM maps for the (D) early closed and (E) fully closed conformations of γTuRC, highlighting positions 1, 2, and 14. The black arrowheads indicate the regions where the positions (D) are not fully in contact and (E) establish lateral contacts. Insets show representative 2D averages of the particles for each conformation (scale bars, 10 nm).

fully closed conformation was sufficient to make a model of its structural organization (Fig. 5C, right panel). This fully closed γTuRC structure was compared with the structure of a 13-protofilament microtubule filtered at a similarly low resolution that, however, still allowed us to see the position and shape of each α/β-tubulin heterodimer (Fig. 5C and fig. S8, D and E). From this comparison and by measuring the distance between the last γ-tubulin in position 14 and its neighboring α-tubulin, we find that the early closed conformation achieves 67% of the extent of closure achieved by the fully closed conformation. In contrast to both the open and early closed conformations of γTuRC, the fully closed conformation matches the geometry of the microtubule so that the 13 γ-tubulins (from positions 2 to 14) can serve as a template with the correct helical pitch for microtubule nucleation (Fig. 5C), establishing the structural basis for γTuRC to nucleate precisely 13-protofilament microtubules in human cells.

Discussion

In this study, we solved the structure of a γTuRC as it nucleates a microtubule at ~4-Å resolution (movies S6 and S7). Key to achieving this resolution was increasing the nucleation efficiency of purified human γTuRC—which is typically in a poorly active, open conformation (*27*, *34*)—to essentially 100% but at the same time keeping microtubules very short. Our structure shows how the complex undergoes a major conformational change as the length of the nucleated microtubule increases to become a perfect template for the nucleation of microtubules with precisely 13 protofilaments, as present in the cytoplasm of human cells.

Comparing the fully closed structure with the early closed and the open structures of γTuRC reveals concerted structural changes of all GCP subunits that are induced by the addition of α/β-tubulin heterodimers. Closure of the γ-tubulin "ring" places GCP3 in position 14, precisely overlapping with GCP2 in position 1 and hindering nucleation at this first position. This arrangement of GCP subunits explains why human γTuRC serves as a perfect template for 13-protofilament microtubules—one of its key functions—despite exposing 14 γ-tubulins in its open conformation before nucleation. Our observations agree with recently reported lower-resolution cryo-EM structures of closed conformations of human and yeast γTuRC, which are, however, attached to 13-protofilament microtubules of considerably greater length than in our study (*46*, *47*). The perfect match of the postnucleation γTuRC and microtubule structures also provides an explanation for the exceptional stability of their interface, as observed

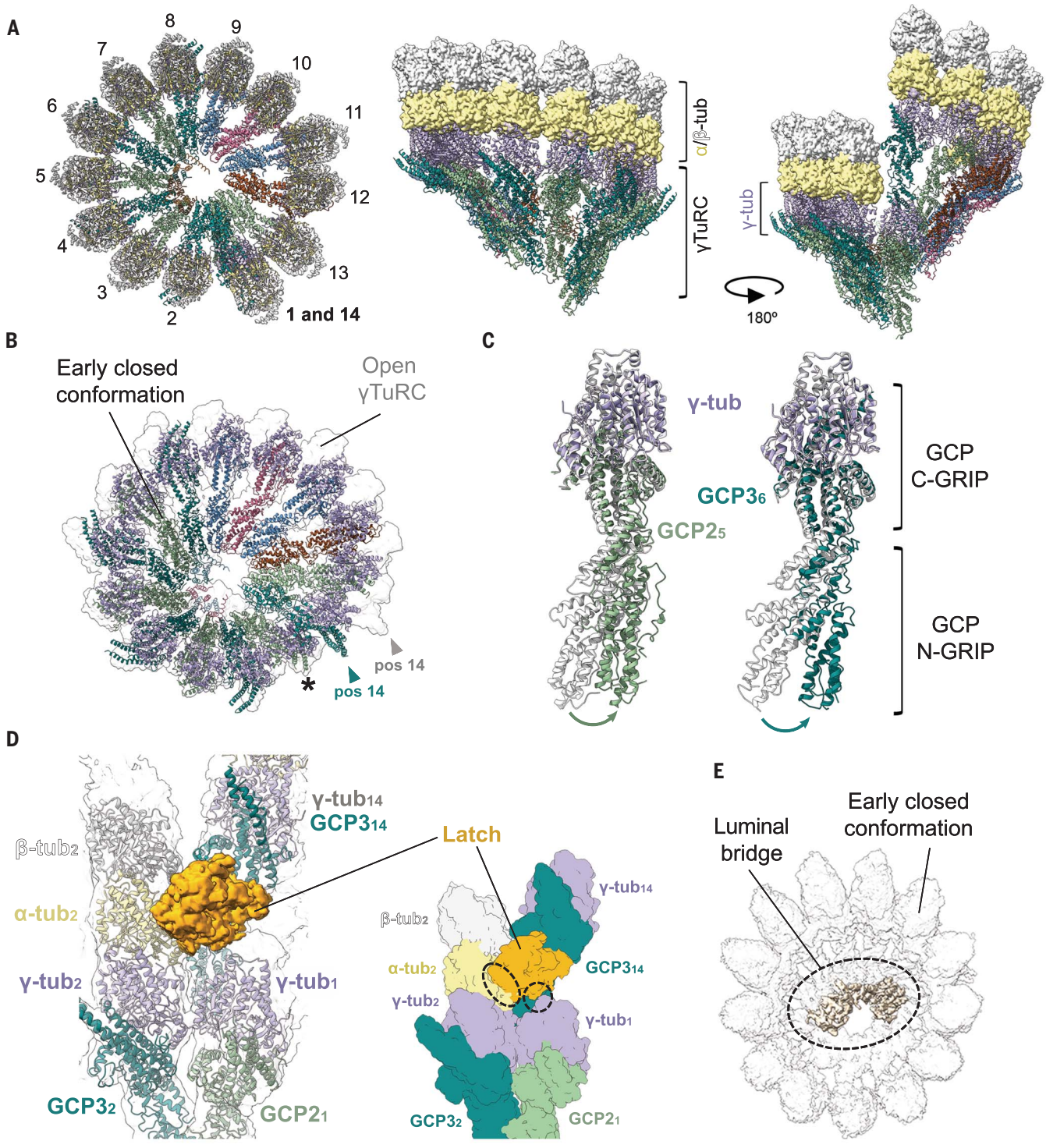

Fig. 4. Structure of γTuRC-nucleated microtubules. (**A**) Top (left panel) and two side views (middle and right panels) of the structure of the early closed conformation of microtubule nucleating γTuRC. γTuRC is represented in ribbons, while the α/β-tubulin heterodimers are displayed as a surface. Each protein subunit is color coded as in Fig. 3B. (**B**) Top view of the early closed conformation superimposed with the contour of the structure of the open γTuRC (white), both aligned using position 1 as a reference (asterisk). The movement of position 14 when the ring closes is indicated. (**C**) Conformational changes undergone in the γTuRC subunits $GCP2_5$ and $GCP3_6$ upon microtubule nucleation (color coded as in Fig. 3B) and with respect to the open γTuRC conformation (white ribbons). The structures of the subunits were aligned on the basis of the γ-tubulin position. The arrows indicate the conformational movement. GCP C-GRIP and N-GRIP domains are indicated. (**D**) Latch density (orange surface, left panel) interacting with γ-tubulin in position 1 of the γTuRC and with the α/β-tubulin heterodimer in position 2. The dashed circles in the cartoon (right panel) highlight the interfaces of contact between the different elements with the latch (orange). (**E**) Luminal density in the early closed conformation of microtubule nucleating γTuRC is highlighted with a dashed ellipse (beige density) within the corresponding cryo-EM structure (white surface).

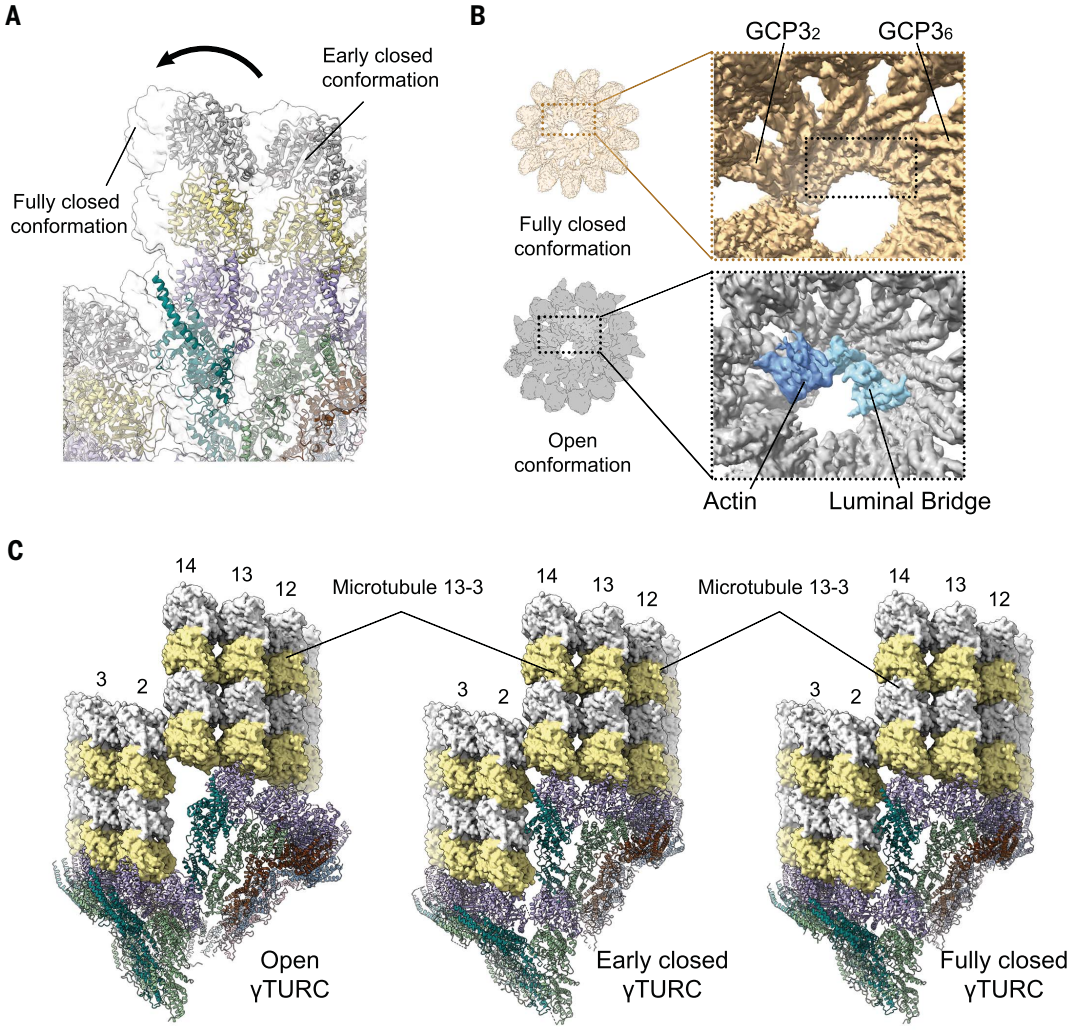

Fig. 5. Fully closed γTuRC is a template for 13-protofilament microtubules. (**A**) Structure of the early closed γTuRC (color coded as in Fig. 3B) superimposed with the surface of the fully closed conformation (white). Arrow indicates the movement of the α/β-tubulin heterodimers on top of the last GCP pair from the early to the fully closed conformation. (**B**) The fully closed conformation of microtubule nucleating γTuRC lacks density for both actin and the MZT1-NTE modules of the luminal bridge (top panel), unlike the open γTuRC conformation where both the actin and the luminal bridge (highlighted in blue) are evident (bottom panel). A cartoon representation of each γTuRC conformation is included for reference. (**C**) Structures of the open (left panel, PDB ID 7AS4), closing (middle panel), and fully closed (right panel) γTuRC conformation superimposed with the structure of a 13-protofilament microtubule (EMD-5193), where the surface of two layers of α/β-tubulins are shown on top of each γTuRC conformation. To help visualization, both the microtubule model and the γTuRC structures were sliced, showing only the front of the structures, and some of the γTuRC and protofilament positions are indicated. Distance between the Asn[187] residue of the γ-tubulin in position 14 and the conserved Asn[186] residue of the adjacent α-tubulin (located in the second layer of α/β-tubulin at position 2) was measured for the open (~110 Å), early closed (~84 Å), and fully closed (~71 Å) γTuRC conformations and served to estimate the degree of γTuRC ring closure.

in vitro (*27*, *34*, *36*, *48*–*50*), suggesting that energy-consuming destabilizing activities, such as those of severases and depolymerases, may be needed in cells to recycle the complex for additional rounds of nucleation, consistent with recent in vitro reconstitutions (*49*) and observations in cells (*51*, *52*).

The movement toward closure is promoted by a latch extending from the last GCP3 at position 14, a part of γTuRC that has been previously described as an "end protrusion" in the open conformation of human γTuRC, possibly representing another MZT1-like/NTE module (*28*–*31*, *35*). Our structure now suggests the function of this end protrusion as it interacts like a latch with both γ-tubulin in position 1 and the α/β-tubulin heterodimer at position 2, at the base of the microtubule seam. Therefore, tubulin incorporation at the seam becomes an integral part of the closing mechanism mediated by this latch, ensuring the 13-fold symmetry of the template. The importance of the involvement of α/β-tubulin for conformational closure is also supported by the recent observation of only partial closure of the complex in the absence of tubulin when the γTuRC-activating CM1 domain binds to the complex (*53*). When the nucleated microtubule is sufficiently long and the γTuRC is in its fully closed conformation, the latch no longer appears to be required to maintain the closed state (fig. S4).

Once γTuRC is closed, the actin and MZT1/NTE modules forming the luminal bridge are not found in the lumen of the complex. Their absence is consistent with the proposal that the MZT1/NTE modules are important for stabilizing the γTuRC structure during complex assembly in its open conformation (*34*). The actin molecule may however be dispensable for complex assembly (*35*), and its role for γTuRC-mediated microtubule nucleation has remained unclear (*35*). Actin in the vicinity of the GCPs at positions 2 and 3 could be an obstacle for the full closure of the γTuRC given that the space required to accommodate it becomes much reduced and actin could partially clash with GCP3 in position 14 in the closing complex. We find that actin indeed leaves the center of the complex, either being ejected from γTuRC or delocalized to another region, for full closure, opening the possibility of actin incorporation in the luminal bridge having a negative regulatory role. This possibility may support the notion of cross-talk between the actin and microtubule cytoskeleton as recently proposed for microtubule and actin filament nucleation at centrosomes (*54*, *55*). This will be an interesting direction for future research.

The activity of budding yeast γTuRC appears to be mostly regulated by its assembly on the spindle pole body, where it adopts a structure that is already a relatively good match with the microtubule structure (*19*, *56*). Nevertheless, a final conformational closure step is also required in this organism to form a perfect template (*23*, *47*). In contrast, vertebrate γTuRC

has evolved to assemble in the cytoplasm in a conformation that deviates considerably from the microtubule structure, probably to maintain a low basal level of activity. Larger-scale rearrangements are required for vertebrate γTuRC to adopt its functional templating conformation.

Regulators that directly bind to γTuRC, such as the anchoring protein CDK5RAP2 at centrosomes, may directly affect closure of the complex, thereby enhancing nucleation (*50*, *57*, *58*). Closure may be promoted by facilitating the required conformational changes of the latch, removing the luminal bridge, or promoting the concerted conformational changes of the GCPs as observed in the closed γTuRC structure. Alternatively, regulators acting on microtubule growth, such as the microtubule polymerase chTOG (*27*, *59*, *60*), or an enhanced tubulin concentration at centrosomes (*61*) may stimulate γTuRC closure by promoting the growth of a nascent microtubule on the complex. Future structural work will reveal the mechanisms by which distinct regulators control the activity of the complex by modulating its conformational changes to ensure the correct levels of nucleation activity at the right place and time.

REFERENCES AND NOTES

1. E. Nogales, M. Whittaker, R. A. Milligan, K. H. Downing, *Cell* **96**, 79–88 (1999).
2. E. Nogales, R. Zhang, *Curr. Opin. Struct. Biol.* **37**, 90–96 (2016).
3. S. W. Manka, C. A. Moores, *Essays Biochem.* **62**, 737–751 (2018).
4. E. M. Mandelkow, R. Schultheiss, R. Rapp, M. Müller, E. Mandelkow, *J. Cell Biol.* **102**, 1067–1073 (1986).
5. R. H. Wade, D. Chrétien, D. Job, *J. Mol. Biol.* **212**, 775–786 (1990).
6. J. R. Simon, E. D. Salmon, *J. Cell Sci.* **96**, 571–582 (1990).
7. S. Chaaban, G. J. Brouhard, *Mol. Biol. Cell* **28**, 2924–2931 (2017).
8. L. G. Tilney *et al*., *J. Cell Biol.* **59**, 267–275 (1973).
9. S. Ray, E. Meyhöfer, R. A. Milligan, J. Howard, *J. Cell Biol.* **121**, 1083–1093 (1993).
10. J. Kraus, R. Alfaro-Aco, B. Gouveia, S. Petry, *Trends Biochem. Sci.* **48**, 761–775 (2023).
11. P. Liu, M. Würtz, E. Zupa, S. Pfeffer, E. Schiebel, *Curr. Opin. Cell Biol.* **68**, 124–131 (2021).
12. Y. Zheng, M. L. Wong, B. Alberts, T. Mitchison, *Nature* **378**, 578–583 (1995).
13. M. Moritz, M. B. Braunfeld, J. W. Sedat, B. Alberts, D. A. Agard, *Nature* **378**, 638–640 (1995).
14. M. Moritz, Y. Zheng, B. M. Alberts, K. Oegema, *J. Cell Biol.* **142**, 775–786 (1998).
15. C. Wiese, Y. Zheng, *Nat. Cell Biol.* **2**, 358–364 (2000).
16. T. J. Keating, G. G. Borisy, *Nat. Cell Biol.* **2**, 352–357 (2000).
17. M. Moritz, M. B. Braunfeld, V. Guénebaut, J. Heuser, D. A. Agard, *Nat. Cell Biol.* **2**, 365–370 (2000).
18. J. M. Kollman *et al*., *Mol. Biol. Cell* **19**, 207–215 (2008).
19. J. M. Kollman, J. K. Polka, A. Zelter, T. N. Davis, D. A. Agard, *Nature* **466**, 879–882 (2010).
20. K. Oegema *et al*., *J. Cell Biol.* **144**, 721–733 (1999).
21. M. Knop, G. Pereira, S. Geissler, K. Grein, E. Schiebel, *EMBO J.* **16**, 1550–1564 (1997).
22. S. Geissler *et al*., *EMBO J.* **15**, 3899–3911 (1996).
23. J. M. Kollman *et al*., *Nat. Struct. Mol. Biol.* **22**, 132–137 (2015).
24. S. M. Murphy, L. Urbani, T. Stearns, *J. Cell Biol.* **141**, 663–674 (1998).
25. S. M. Murphy *et al*., *Mol. Biol. Cell* **12**, 3340–3352 (2001).
26. V. Guillet *et al*., *Nat. Struct. Mol. Biol.* **18**, 915–919 (2011).
27. T. Consolati *et al*., *Dev. Cell* **53**, 603–617.e8 (2020).
28. P. Liu *et al*., *Nature* **578**, 467–471 (2020).
29. M. Wieczorek *et al*., *Cell* **180**, 165–175.e16 (2020).
30. F. Zimmermann *et al*., *Sci. Adv.* **6**, eabe0894 (2020).
31. M. Wieczorek, T. L. Huang, L. Urnavicius, K. C. Hsia, T. M. Kapoor, *Cell Rep.* **31**, 107791 (2020).
32. A. Böhler *et al*., *BioEssays* **43**, e2100114 (2021).
33. A. Merdes, *J. Cell Biol.* **220**, e202101015 (2021).
34. M. Wieczorek *et al*., *J. Cell Biol.* **220**, e202009146 (2021).
35. M. Würtz *et al*., *Nat. Commun.* **13**, 473 (2022).
36. A. Thawani *et al*., *eLife* **9**, e54253 (2020).
37. J. Roostalu *et al*., *eLife* **9**, e51992 (2020).
38. Y. Komarova *et al*., *J. Cell Biol.* **184**, 691–706 (2009).
39. L. Pecqueur *et al*., *Proc. Natl. Acad. Sci. U.S.A.* **109**, 12011–12016 (2012).
40. P. Bieling *et al*., *J. Cell Biol.* **183**, 1223–1233 (2008).
41. P. Bieling *et al*., *Nature* **450**, 1100–1105 (2007).
42. E. D. Zhong, T. Bepler, B. Berger, J. H. Davis, *Nat. Methods* **18**, 176–185 (2021).
43. A. Punjani, J. L. Rubinstein, D. J. Fleet, M. A. Brubaker, *Nat. Methods* **14**, 290–296 (2017).
44. R. Fernandez-Leiro, S. H. W. Scheres, *Acta Crystallogr. D Struct. Biol.* **73**, 496–502 (2017).
45. J. Zivanov *et al*., *eLife* **11**, e83724 (2022).
46. A. Aher, L. Urnavicius, A. Xue, K. Neselu, T. Kapoor, bioRxiv 2023.11.20.567916 [Preprint] (2023); https://doi.org/10.1101/2023.11.20.567916.
47. D. Barford *et al*., Research Square [Preprint] (2023); https://doi.org/10.21203/rs.3.rs-3481382/v1.
48. A. Y. Berman *et al*., *J. Cell Biol.* **222**, e202204102 (2023).
49. G. Henkin, C. Brito, C. Thomas, T. Surrey, *J. Cell Biol.* **222**, e202304020 (2023).
50. D. Rai *et al*., bioRxiv 2022.08.03.502613 [Preprint] (2022); https://doi.org/10.1101/2022.08.03.502613.
51. T. J. Keating, J. G. Peloquin, V. I. Rodionov, D. Momcilovic, G. G. Borisy, *Proc. Natl. Acad. Sci. U.S.A.* **94**, 5078–5083 (1997).
52. A. Laguillo-Diego *et al*., *Mol. Biol. Cell* **34**, ar1 (2023).
53. Y. Xu *et al*., bioRxiv 2023.12.14.571518 [Preprint] (2023); https://doi.org/10.1101/2023.12.14.571518.
54. F. Farina *et al*., *EMBO J.* **38**, e99843 (2019).
55. D. Inoue *et al*., *EMBO J.* **38**, e99630 (2019).
56. M. Knop, E. Schiebel, *EMBO J.* **17**, 3952–3967 (1998).
57. Y. K. Choi, P. Liu, S. K. Sze, C. Dai, R. Z. Qi, *J. Cell Biol.* **191**, 1089–1095 (2010).
58. M. J. Rale, B. Romer, B. P. Mahon, S. M. Travis, S. Petry, *eLife* **11**, e80053 (2022).
59. J. Roostalu, N. I. Cade, T. Surrey, *Nat. Cell Biol.* **17**, 1422–1434 (2015).
60. A. Ali, C. Vineethakumari, C. Lacasa, J. Lüders, *Nat. Commun.* **14**, 289 (2023).
61. J. B. Woodruff *et al*., *Cell* **169**, 1066–1077.e10 (2017).

ACKNOWLEDGMENTS

We thank R. Garcia-Castellanos and S. Speroni for technical assistance, F. Ruhnow for microscopy support, and the Cell Services of the Francis Crick Institute, London, UK, for producing large HeLa cell cultures with tagged γTuRC. We thank J. Boskovic and J. LeCoq from the CNIO Electron Microscopy Unit (CNIO, Spain) for help with cryo-EM and R. Fernandez-Leiro and N. Gonzalez-Rodriguez (CNIO, Spain) for advice during image processing and modeling. We thank the Basque Resource for Electron Microscopy (BREM) and D. Gil-Carton for the help with the cryo-EM data used in this work. We thank the IBMB CSIC Cryo-EM Platform staff for assistance during the microscope data acquisition. **Funding:** Work in the Surrey lab was supported by the Spanish Ministry of Science and Innovation through the Centro de Excelencia Severo Ochoa (CEX2020-001049-S, MCIN/AEI/10.13039/501100011033) and the Generalitat de Catalunya through the CERCA program. T.S. also acknowledges support from the European Research Council (ERC Synergy Grant, Project 951430) and from the Spanish Ministry of Science and Innovation (grant PID2019-108415GB-I00). C.B. was supported by EMBO long-term fellowship ALTF-883-2020 and Marie Curie fellowship TuRCReg. Work in the Llorca lab was funded by the Agencia Estatal de Investigación (AEI/10.13039/501100011 033) and the Ministerio de Ciencia e Innovación (PID2020-114429RB-I00 to O.L.). The Llorca lab also received support from the National Institute of Health Carlos III to CNIO. The IBMB-CSIC Cryo-EM Platform is supported by project IU16-014045 (CRYO-TEM) from Generalitat de Catalunya and by "ERDF A way of making Europe" from the European Union. Part of this work was performed at the Basque Resource for Electron Microscopy located at Instituto Biofisika (UPV/EHU, CSIC), supported primarily by the Department of Education and the Innovation Fund of the Basque Government, with additional support from Fundación Biofísica Bizkaia and MCIN with funding from European Union NextGenerationEU (PRTR-C17.I1). **Author contributions:** C.B. purified the proteins and carried out the assays to characterize γTuRC-mediated microtubule nucleation. C.B., M.S., and P.G. performed cryo-EM experiments. M.S. performed image processing, structural determination, and analysis. C.B., M.S., O.L., and T.S. designed the research. C.B., M.S., O.L., and T.S. prepared the manuscript. **Competing interests:** The authors declare that they have no competing interests. **Data and materials availability:** Cryo-EM map and refined coordinates of the early closed conformation of the microtubule nucleating γTuRC were deposited in the Electron Microscopy Data Bank (EMDB) with accession code EMD-18181 and in the Protein Data Bank (PDB) under PDB ID 8Q62. The EMD-18181 entry also includes the volumes of the intermediate states obtained using cryoDRGN. The cryo-EM map of the fully closed conformation of the microtubule nucleating γTuRC was deposited in the EMDB with accession code EMD-18182. The structural model for the fully closed conformation made by flexible fitting into the cryo-EM map is available in the supplementary materials. This research was funded in whole or in part by the European Research Council (ERC Synergy Grant, Project 951430). The author will make the Author Accepted Manuscript (AAM) version available under a CC BY public copyright license.

SUPPLEMENTARY MATERIALS

science.org/doi/10.1126/science.adk6160
Materials and Methods
Figs. S1 to S8
Table S1
References (*62*–*81*)
MDAR Reproducibility Checklist
Movies S1 to S7
Data S1

Submitted 1 September 2023; accepted 22 January 2024
Published online 1 February 2024
10.1126/science.adk6160